

# Optical interferometry of early-type stars with PAVO@CHARA – I. Fundamental stellar properties

V. Maestro,<sup>1</sup>\* X. Che,<sup>2</sup> D. Huber,<sup>1,3</sup> M. J. Ireland,<sup>1,4,5</sup> J. D. Monnier,<sup>2</sup> T. R. White,<sup>1</sup>  
Y. Kok,<sup>1</sup> J. G. Robertson,<sup>1</sup> G. H. Schaefer,<sup>6</sup> T. A. Ten Brummelaar<sup>6</sup> and P. G. Tuthill<sup>1</sup>

<sup>1</sup>Sydney Institute for Astronomy, School of Physics, University of Sydney, NSW 2006, Australia

<sup>2</sup>Astronomy Department, University of Michigan, 941 Denison Bldg, Ann Arbor, MI 48109-1090, USA

<sup>3</sup>NASA Ames Research Center, Moffett Field, CA 94035, USA

<sup>4</sup>Department of Physics and Astronomy, Macquarie University, NSW 2109, Australia

<sup>5</sup>Australian Astronomical Observatory, PO Box 915, North Ryde, NSW 1670, Australia

<sup>6</sup>Center for High Angular Resolution Astronomy, Georgia State University, PO Box 3969, Atlanta, GA 30302, USA

Accepted 2013 June 14. Received 2013 June 13; in original form 2013 April 25

## ABSTRACT

We present interferometric observations of seven main-sequence and three giant stars with spectral types from B2 to F6 using the Precision Astronomical Visible Observations beam combiner at the Center for High Angular Resolution Astronomy array. We have directly determined the angular diameters for these objects with an average precision of 2.3 per cent. We have also computed bolometric fluxes using available photometry in the visible and infrared wavelengths, as well as space-based ultraviolet spectroscopy. Combined with precise *Hipparcos* parallaxes, we have derived a set of fundamental stellar properties including linear radius, luminosity and effective temperature. Fitting the latter to computed isochrone models, we have inferred masses and ages of the stars. The effective temperatures obtained are in good agreement (at a 3 per cent level) with nearly independent temperature estimations from spectroscopy. They validate recent sixth-order polynomial  $(B - V) - T_{\text{eff}}$  empirical relations, but suggest that a more conservative third-order solution could adequately describe the  $(V - K) - T_{\text{eff}}$  relation for main-sequence stars of spectral types A0 and later. Finally, we have compared mass values obtained combining surface gravity with inferred stellar radius (*gravity mass*) and as a result of the comparison of computed luminosity and temperature values with stellar evolutionary models (*isochrone mass*). The strong discrepancy between isochrone and gravity masses obtained for one of the observed stars,  $\gamma$  Lyr, suggests that determination of the stellar atmosphere parameters should be revised.

**Key words:** techniques: interferometric – stars: early-type – stars: fundamental parameters.

## 1 INTRODUCTION

Long-baseline optical interferometry (with baselines up to hundreds of metres in length) has enabled us to measure angular diameters of bright stars, with typical values of a few milliarcseconds. Combined with accurate parallax and photometry, these measurements allow direct determination of fundamental stellar properties, such as the linear radii of their photospheres or the effective surface temperature of the stars, and have become a very valuable tool to contrast observational results with stellar models of increasing complexity.

The pioneering work of Hanbury Brown, Davis & Allen (1974a), using the Narrabri Stellar Intensity Interferometer (NSII), provided angular sizes of 32 O- to F-type stars. Subsequently, Code et al.

(1976) established the empirical temperature scale for stars of spectral type F5 and earlier by means of combining Hanbury Brown et al. (1974a) diameters with multiband spectra from which they inferred bolometric fluxes. The majority of the stars observed with the NSII belonged to luminosity classes I–III, and only about one third of them were main-sequence or subgiant stars (luminosity classes IV or V), since the instrument favoured observations of stars with larger diameters, given the same surface brightness. For several decades, all the early-type-star (between O0 and A7) diameter measurements (a total of 16) came from the NSII observations (Davis 1997). Even in more recent years, the papers referenced in the Catalog of High Angular Resolution Measurements (CHARM2) catalogue (Richichi, Percheron & Khristoforova 2005) contained just 24 entries corresponding to direct diameter measurements for main-sequence or subgiant stars. The advent of optical long-baseline interferometry using hectometric baselines, particularly

\*E-mail: V.Maestro@physics.usyd.edu.au

in the near-infrared, has provided rapid progress in the number of main-sequence and subgiant stars with direct diameter measurements. Most notably, van Belle & von Braun (2009) reported interferometric diameter measurements for 44 G-type or later main-sequence stars, deriving colour–temperature relations, and Boyajian et al. (2012a,b) published results of a survey carried out on a combined sample of 77 dwarfs spanning from A to M spectral types, developing new empirical laws relating broad-band colours and effective temperature.

As a result of resolution and sensitivity constraints particularly in the near-infrared, there is a clear sample bias, as only 5 out of the 121 stars studied in these papers belong to spectral class A or earlier. The major stumbling block has been that to access significant populations of hot stars, resolutions better than 1 mas are required. The rise of beam combiners that can operate in the visible range of the spectrum with improved sensitivity, such as Precision Astronomical Visible Observations (PAVO)@ Center for High Angular Resolution Astronomy (CHARA), allows routine measurements of submilliarcsecond stellar diameters (Huber et al. 2012a; White et al. 2013) and offers the possibility to extend the spectral range to earlier type stars within similar sensitivity constraints.

Obtaining precise individual properties of B and A main-sequence stars is of considerable importance in stellar astrophysics, since they represent the most massive and luminous objects that can be described by models containing simplifying assumptions such as local thermodynamic equilibrium physics, hydrostatic equilibrium or purely radiative envelopes, in contrast to those corresponding to more massive or evolved objects, providing a useful benchmark for stellar atmosphere models. Furthermore, the intrinsic higher surface brightness of early-type (mainly B and A) stars makes them suitable calibration stars (Boden 2003; Mozurkewich et al. 2003) for correction of instrumental and atmospheric effects in visible and near-infrared interferometry. Therefore, direct measurement of submilliarcsecond angular stellar diameters has the potential to improve calibration of interferometric observations of objects with larger projected sizes.

The drawback is that stars earlier than F6 often rotate rapidly (van Belle 2012). As the rotational velocity approaches its critical value, the centrifugal force induces latitudinal temperature gradients (an

effect known as *gravity darkening*, von Zeipel 1924a,b; Maeder & Meynet 2000) and, depending on the inclination of the stellar rotation axis, the apparent stellar disc may look oblate. Projected rotational velocities can be used to model the effect of rotation in the interferometric observables (Yoon et al. 2007), with the finding that effects of low rotation rates can be neglected for low spatial frequencies.

In this paper, we present the results of our pilot study on a small sample of 10 nearby stars with submilliarcsecond angular size with spectral types in the B2–F6 range. Computed bolometric fluxes, together with precise *Hipparcos* parallaxes, have been used to derive the fundamental stellar parameter’s linear radius, luminosity and effective temperature, with results that are in good agreement with measurements obtained using independent methods. Finally, we have estimated stellar mass and ages by means of isochrone model fitting.

## 2 TARGET SAMPLE AND OBSERVATIONS

### 2.1 Target sample

The stars observed in our study are extensively used as calibrators in near-infrared interferometry, mainly in observations using the Michigan InfraRed Combiner instrument (see, e.g., Monnier et al. 2007; Zhao et al. 2009; Che et al. 2011). In addition to their use in fundamental parameters of the observed stars (in combination with other measurements), angular diameter estimation constitutes a direct measurement of the interferometric response independent of diameter estimates based on indirect methods (see Cruzalèbes et al. 2010, and references therein) that rely on high-fidelity spectral energy distribution (SED) templates or stellar atmosphere models.

Table 1 lists the objects observed, as well as the physical parameters describing their stellar atmospheres ( $T_{\text{eff}}$ ,  $\log g$  and metallicity), determined from spectroscopic and photometric observations. It also includes the measured *Hipparcos* parallaxes (van Leeuwen 2007). These parallaxes correspond to distances smaller than  $\sim 200$  pc, with uncertainties ranging from 1 to 5 percent for most of the stars observed. The more distant stars  $\sigma$  Cyg and  $o$  And

**Table 1.** Physical parameters of the stars presented in this work. The objects are separated into main-sequence and subgiant stars (top), and giants and supergiants (bottom) in ascending temperature order.

Name	HD	SpTy	Photometry			Atmosphere parameters			<i>Hipparcos</i> $\pi$ (mas)	Rotation $v \sin i$
			$V$	$B-V$	$V-K$	$T_{\text{eff}}$	$\log g$	[Fe/H]		
40 Leo	HD 89449 <sup>a, b</sup>	F6IV–V	4.8	0.44	1.140	6447 ± 40	4.11 ± 0.02	0.09 ± 0.03	46.8 ± 0.24	17 ± 2
7 And	HD 219080 <sup>d, k</sup>	F1V	4.54	0.279	0.753	7292 ± 127	4.16 ± 0.02	−0.02 ± 0.08	40.67 ± 0.22	61 ± 6
37 And	HD 5448 <sup>g, h</sup>	A6V	3.867	0.133	0.365	8090 ± 300	3.99 ± 0.15	0.03 ± 0.05	25.14 ± 0.86	70 ± 11
$\theta$ Leo	HD 97633 <sup>a, b, k, o, p, q, r, s</sup>	A2V	3.324	0.013	0.010	9286 ± 183	3.68 ± 0.15	−0.03 ± 0.13	19.76 ± 0.17	21 ± 4
$b$ Leo	HD 95608 <sup>i, k</sup>	A1V	4.407	0.058	0.092	9372 ± 477	4.22 ± 0.20	0.00 ± 0.10	25.73 ± 0.18	18 ± 7
$\eta$ Aur	HD 32630 <sup>e, l</sup>	B4V	3.158	−0.146	−0.591	16 821 ± 295	4.10 ± 0.02	−0.04 ± 0.07	13.4 ± 0.2	98 ± 25
$\zeta$ Cas	HD 3360 <sup>a, b, f, m, n</sup>	B2IV	3.666	−0.183	−0.849	21 061 ± 706	3.84 ± 0.05	−0.07 ± 0.08	5.5 ± 0.16	17 ± 8
$\gamma$ Lyr	HD 176437 <sup>a, b, f, j, k</sup>	A1III	3.25	−0.05	−0.036	10 959 ± 973	3.81 ± 0.24	0.12 ± 0.03	5.26 ± 0.27	65 ± 12
$\sigma$ Cyg	HD 202850 <sup>b</sup>	B9.5Ia	4.256	0.086	0.003	11 839 ± 256	2.05 ± 0.06	0.15 ± 0.13	1.13 ± 0.19	25 ± 10
$o$ And	HD 217675 <sup>c</sup>	B6III	3.633	−0.081	−0.360	14 491 ± 435	2.95 ± 0.10	0.03 ± 0.14	4.75 ± 0.53	240 ± 50

*Notes.*  $V$  magnitude and  $(B - V)$  colour are taken from references in SIMBAD.  $(V - K)$  colour computed using  $K$ -band photometry is taken from the General Catalogue of Photometric Data (GCPD; Mermilliod, Mermilliod & Hauck 1997). Stellar atmosphere parameters for every object have been averaged over the values presented in <sup>a</sup>Prugniel, Vauglin & Koleva (2011), <sup>b</sup>Wu et al. (2011), <sup>c</sup>Pier, Saha & Kinman (2003), <sup>d</sup>Ersparmer & North (2003), <sup>e</sup>Fitzpatrick & Massa (2005), <sup>f</sup>Koleva & Vazdekis (2012), <sup>g</sup>Blackwell & Lynas-Gray (1998), <sup>h</sup>Gardiner, Kupka & Smalley (1999), <sup>i</sup>Allende Prieto & Lambert (1999), <sup>j</sup>Balachandran et al. (1986), <sup>k</sup>Ammons et al. (2006), <sup>l</sup>Adelman et al. (2002), <sup>m</sup>Gies & Lambert (1992), <sup>n</sup>Nieva & Przybilla (2012), <sup>o</sup>Adelman (1986), <sup>p</sup>Adelman (1988), <sup>q</sup>Cottrell & Sneden (1986), <sup>r</sup>Hill & Landstreet (1993), <sup>s</sup>Smith & Dworetzky (1993). Parallaxes are taken from van Leeuwen (2007). Projected rotational velocities ( $v \sin i$ ) are taken from Głębocicki & Gnański (2005).

have larger 17 and 11 per cent errors at a distance of 880 and 210 pc, respectively.

The stars in our sample span from B2 to F6 spectral types (effective temperatures in the 21 000–6400 K range). Most of them (seven) are main sequence or subgiants (luminosity classes V or IV), two are giants ( $\gamma$  Lyr,  $\sigma$  And) and one is a supergiant star ( $\sigma$  Cyg). Main-sequence stars of spectral types earlier than  $\sim$ F6 ( $M > 1.5 M_{\odot}$ ), exhibiting radiative envelopes, are expected to rotate rapidly (see van Belle 2012, and references therein). As a consequence, they can show significant projected oblateness depending on the inclination of their polar axis. All the stars in our sample, with the sole exception of  $\sigma$  And ( $v \sin i \sim 250 \text{ km s}^{-1}$ , see Balona & Dziembowski 1999; Głęboccki & Gnaniński 2005), have projected rotational velocities that are significantly less than 50 per cent of the critical rotational velocity (see typical values for different spectral types in Tassoul 2000), and therefore no important deviations from projected circular shapes are expected (Frémat et al. 2005). For  $\sigma$  And, Clark, Tarasov & Panko (2003) reported that  $\sigma$  And could be seen nearly equator-on, implying that the star rotates at  $\sim$ 50 per cent of the critical velocity, which would result in an equatorial radius less than 4 per cent larger than the polar radius (Owocki, Cranmer & Blondin 1994). Unfortunately, our observations are not sensitive to oblateness, given that we observed this object using only one baseline.

Among the stars studied, three objects ( $\sigma$  Cyg,  $b$  Leo and  $\sigma$  And) present some hints for the existence of companions at less than  $1^{\circ}$  in separation according to the Eggleton & Tokovinin (2008) compilation. Nevertheless, only one object ( $\sigma$  And) shows observational evidence of the existence of close companions according to the Washington Double Star catalogue (Mason et al. 2001), the Multiple Star Catalogue (Tokovinin 1997) and the 9th Catalogue of Spectroscopic Binary Orbits (Pourbaix et al. 2004).  $\sigma$  And is a complex object, consisting of two components A and B (Olević & Cvetković 2006), separated by 0.34 arcsec [ $m_V(A) = 3.63$ ;  $m_V(B) = 6.03$ ]. Both components have been described as spectroscopic binaries. The Aa–Ab components of the main spectroscopic binary have an estimated separation of 0.05 arcsec. The brightest star of the pair is believed to be a  $\gamma$  Cas-type variable that injects material in a circumstellar shell in rapid discrete ejections (Clark et al. 2003), switching between Be- and B-type spectra in a time-scale of  $\sim 10^3$  d. The short-term photometric variability of this object does not correlate with an enhancement in the shell emission and seems to be photospheric in origin. All these features make  $\sigma$  And an extraordinarily difficult object to study, with conditions that might be relatively far from the simplified assumptions (circular projected shape and isothermal surface) considered throughout this paper; its continued use as an interferometric calibrator is not advised. Nevertheless, the measured angular diameter and effective temperature of  $\sigma$  And show that the influence of companion objects is smaller than the precision of our observations.

## 2.2 Interferometry

Interferometric observations of our target sample were carried out using the PAVO beam combiner (Ireland et al. 2008), located at the CHARA array (ten Brummelaar et al. 2005) on Mt Wilson Observatory (CA, USA). The CHARA array is an optical interferometer, consisting of six 1 m telescopes arranged in a Y-shaped configuration. Operating in visible and infrared wavelengths, it provides a total of 15 different baselines at different orientations with lengths in the range 34–331 m. With the longest operational baselines available in the world provided by the CHARA array and the use of visible light (0.6–0.9  $\mu\text{m}$ ) in PAVO, the instrumentation used in this

study delivers the highest angular resolution yet achieved ( $\sim$ 0.3 mas in the visible).

The PAVO instrument (see detailed description in Ireland et al. 2008) is a pupil-plane Fizeau beam combiner optimized for sensitivity and high angular resolution. We briefly summarize the basics of the instrument here. Visible and infrared light are separated by a dichroic with a cutoff at 1  $\mu\text{m}$ . The visible beams (up to three) enter PAVO, and are focused by a set of achromatic lenses in an image plane. The beams are passed through a three-hole non-redundant mask that acts as a spatial filter. After going through the mask, the beams interfere and produce spatially modulated pupil-plane fringes. The fringes are formed on a lenslet array that divides the pupil in 16 independent segments, allowing an optimal usage of the multi- $r_0$  apertures of the CHARA array. Finally, a prism disperses the fringes and these are reimaged and recorded on a low-noise readout EMCCD detector. Early PAVO@CHARA results have been presented by Bazot et al. (2011), Derekas et al. (2011) and Huber et al. (2012a,b).

Observations of the objects listed in Table 1 using PAVO@CHARA were carried out in 2010 July (2 and 3), 2011 May (12 and 13), 2011 August (11), 2011 October (2 and 3), 2012 August (5 and 6) and 2012 September (7). Most of the observations were done using one baseline (two telescopes) at a time, with the only exception of  $\sigma$  Cyg, that has also been observed in three-telescope (using the S2E2W2 triangle) mode, allowing simultaneous data collection in three baselines. The baselines used are given in Table 2. Raw interferometric data ( $V^2$ ) were obtained through the use of standard procedures for PAVO@CHARA data (Ireland et al. 2008; Maestro et al. 2012). Some of the objects ( $\zeta$  Cas, 37 And and  $b$  Leo) have been observed on only one night.

Gauging the point-source response of the interferometer is essential to obtain an accurate calibration of the observed sources. To this end, and according to standard practice in optical interferometry (Boden 2003; van Belle & van Belle 2005), we interleave observations of the science targets with others of calibration stars, in such manner that a bracket calibrator–target–calibrator is completed in 15–20 min. The calibration stars match, as closely as possible, the ideal point-like ( $\theta < 0.25$  mas) source located at the smallest angular distance in the sky from the object (at an average distance of  $\sim 7.5$  between target and calibrator). Table 3 shows all the calibrators used in our study. Expected diameters have been computed using  $V - K$  colours (Kervella et al. 2004), dereddened according to the interstellar extinction maps presented by Drimmel, Cabrera-Lavers & López-Corredoira (2003). We have checked each calibrator in the literature for possible multiplicity or variability prior to observations. Analysis of the data obtained for HD 216523 revealed that the object is in fact a binary star, and therefore it was excluded from the list of calibrators. PAVO@CHARA sensitivity limits impose a

**Table 2.** CHARA baselines used. Position angle (PA) is measured in degrees east of north.

Baseline	Length (m)	PA (deg)
W2W1	107.93	−80.9
W2E2	156.26	+63.2
W2S2	177.45	−20.9
W2S1	210.98	−19.1
E2S2	248.13	+17.9
W1S2	249.39	−42.8
W1E2	251.34	+77.7
E1S1	330.70	+22.3

**Table 3.** List of calibration stars used, including the spectral type,  $V - K$  colour and extinction  $E(B - V)$ , the predicted diameter (in milliarcseconds) from  $V - K$  using prescriptions of Kervella et al. (2004) as well as projected rotational velocities ( $v \sin i$ , in  $\text{km s}^{-1}$ ) from Głęboczi & Gnański (2005). Photometry has been taken from references in SIMBAD data base and the GCPD (Mermilliod et al. 1997).

HD	SpTy	$V - K$	$E(B - V)$	$\theta_{V-K}$	$v \sin i$	ID
HD 1279	B7III	-0.157	0.037	0.202	$25 \pm 9$	<i>beg</i>
HD 1606	B7V	-0.358	0.037	0.161	$120 \pm 22$	<i>c</i>
HD 4142	B5V	-0.334	0.034	0.193	$160 \pm 24$	<i>cg</i>
HD 10390	B9V	-0.147	0.007	0.180	$58 \pm 15$	<i>c</i>
HD 29526	A0V	-0.001	0.017	0.243	$80 \pm 13$	<i>f</i>
HD 29721	B9III	0.198	0.037	0.242	$232 \pm 29$	<i>f</i>
HD 88737	F9V	1.334	0.006	0.459	$10 \pm 3$	<i>a</i>
HD 89363	A0	0.117	0.015	0.150	–	<i>ae</i>
HD 92825	A3V	0.155	0.008	0.352	$188 \pm 18$	<i>de</i>
HD 93702	A2V	0.239	0.014	0.326	$208 \pm 15$	<i>de</i>
HD 171301	B8IV	-0.180	0.025	0.184	$53 \pm 15$	<i>h</i>
HD 174262	A1V	0.074	0.025	0.226	$111 \pm 21$	<i>h</i>
HD 174567	A0V	0.073	0.044	0.160	$18 \pm 7$	<i>h</i>
HD 176871	B5V	-0.162	0.038	0.210	$268 \pm 34$	<i>h</i>
HD 179527	B8III	-0.074	0.046	0.208	$30 \pm 12$	<i>h</i>
HD 197392	B8III	-0.21	0.212	0.213	$33 \pm 9$	<i>i</i>
HD 204403	A5V	-0.489	0.027	0.227	$117 \pm 18$	<i>i</i>
HD 207516	B8V	-0.157	0.016	0.179	$103 \pm 18$	<i>i</i>
HD 211211	A2V	0.061	0.018	0.243	$238 \pm 27$	<i>ij</i>
HD 219290	A0V	-0.011	0.023	0.178	$50 \pm 9$	<i>bj</i>
HD 222304	B9V	-0.052	0.024	0.269	$165 \pm 25$	<i>b</i>

Notes. Calibrator not used: HD 216523 (binary star). The last column refers to the ID of the target star for which the calibrator has been used (see the first column of Table 4).

selection bias on the calibration sources, favouring the use of distant late B- to early A-type stars as calibrators, which are prone to show fast rotation and therefore non-circular projected shapes (Domiciano de Souza et al. 2002; van Belle 2012). We circumvent this issue by choosing calibrators with low-projected rotational velocities,  $v \sin i$ , or accounting for an increased uncertainty in the predicted diameter that reflects deviations from the spherical shape (see Section 3). To account for some small correlated instrument systematics that persist after calibration using unresolved sources when the star has been observed only one night, we have included an additional 5 per cent uncertainty to the visibility-squared ( $V^2$ ) errors measured, based on repeated observations of the same object during several nights.

### 3 FUNDAMENTAL STELLAR PARAMETERS

#### 3.1 Angular diameters

The squared-visibility ( $V^2$ ) measurements obtained for each of the stars presented in this work were fitted to the single star limb-darkened disc model (given by Hanbury Brown et al. 1974b)

$$V = \left( \frac{1 - \mu_\lambda}{2} + \frac{\mu_\lambda}{3} \right)^{-1} \left[ (1 - \mu_\lambda) \frac{J_1(x)}{x} + \mu_\lambda \sqrt{\frac{\pi}{2}} \frac{J_{3/2}(x)}{x^{3/2}} \right] \quad (1)$$

with

$$x = \frac{\pi B \theta_{\text{LD}}}{\lambda}, \quad (2)$$

where  $V$  is the visibility,  $\mu_\lambda$  is the linear limb-darkening coefficient,  $J_n(x)$  is the  $n$ th-order Bessel function,  $B$  is the projected baseline,  $\theta_{\text{LD}}$  is the angular diameter after limb-darkening correction and  $\lambda$  is

the wavelength at which the stars are observed. We use  $R$ -band linear limb-darkening coefficients interpolating within the model grid of Claret & Bloemen (2011), using the atmosphere parameters given in Table 1, and assuming a microturbulent velocity of  $2 \text{ km s}^{-1}$ . The values assumed for  $\mu_\lambda$  and its error are the result of taking the median and the 0.158 and 0.842 quantiles of the interpolated values corresponding to  $10^3$  realizations of the normally distributed values of the stellar atmosphere parameters  $T_{\text{eff}}$ ,  $\log g$  and  $[\text{Fe}/\text{H}]$ . The uniform disc diameters were obtained by simply assuming  $\mu_\lambda = 0$  in equation (1). Fig. 1 displays the limb-darkening disc model fitted to the calibrated  $V^2$ . The observations made, as well as the uniform disc (computed assuming  $\mu_R = 0$  in equation 1) and limb-darkened disc diameters estimated, are summarized in Table 4.

Errors in diameter have been estimated through model fitting of equation (1) using synthetic data sets (Derekas et al. 2011; Huber et al. 2012a). These data sets are generated considering the uncertainties in (1) the measured  $V^2$  values for target and calibrators, (2) the adopted PAVO wavelength scale ( $\pm 4.5 \text{ nm}$ ), (3) the calibrator angular sizes ( $\pm 5$  per cent, except those cases where the calibrator is expected to show larger projected oblateness) and (4) linear limb-darkening coefficient (see Table 4). All quantities are assumed to have values that are normally distributed, using  $2 \times 10^4$  simulated data sets for each diameter estimation. Possible correlation between adjacent wavelength channels is also taken into account. The median and the width (derived from the 0.158 and 0.842 quantiles) of the distribution of the fitted diameters give the adopted values for the measured diameter and its uncertainty. The results have been adjusted to assume a reduced- $\chi^2 = 1$ , compensating for underestimation of the squared-visibility error estimates (Berger et al. 2006).

Derived angular diameters show an average precision of 2.3 per cent. Fig. 2 shows the comparison between the measured limb-darkened diameters and different estimations using long-baseline interferometry (CHARM2 meta-catalogue; Harmanec et al. 1996; Vakili et al. 1997; Lane, Boden & Kulkarni 2001), or indirect methods: surface brightness methods and calibrations using colour indices<sup>1</sup> [Jean-Marie Mariotti Center (JMCC) catalogue; Kervella et al. 2004; Lafrasse et al. 2010], and using detailed spectrophotometry in the visible and ultraviolet (Zorec et al. 2009). The overall agreement with other results is good (the average value of  $\theta_{\text{LD}}/\theta_i$  is 0.99 with a scatter of  $\pm 0.06$ ).  $V^2$  data for  $\theta$  Leo do not show evidence of departure from circular shape, although this could be due to the similar orientation, projected on sky, of the baselines used. The stars of earlier spectral types, and particularly  $\sigma$  Cyg,  $\eta$  Aur and  $\zeta$  Cas, depart significantly from the range of spectral types of the stars used to infer Kervella's ( $V - K$ )-diameter relation (A- to K-type), and therefore show larger deviations. It is worth noting the good concordance between observations and predictions made by Zorec et al. (2009).

Second lobe  $V^2$  measurements of  $\theta$  Leo make possible simultaneous estimation of both diameter and linear limb-darkening coefficient  $\mu$  for this object. As a result, we obtain  $\theta(\theta \text{ Leo}) = 0.747 \pm 0.024$  and  $\mu(\theta \text{ Leo}) = 0.47 \pm 0.03$ . This constitutes a modest 1 per cent increment in the estimated diameter, but a remarkable increase in the limb-darkening effect with respect to the fixed  $\mu$  estimation [ $\theta(\theta \text{ Leo}) = 0.740 \pm 0.024$ ;  $\mu(\theta \text{ Leo}) = 0.39 \pm 0.03$ ]. Given the spectral type (A2V) and the low-projected rotational velocity ( $v \sin i \simeq 25 \text{ km s}^{-1}$ ; Royer, Zorec & Gómez 2007),  $\theta$  Leo is likely to be a fast-rotating star viewed nearly pole-on. This results in a higher than expected drop in intensity near the border of the apparent stellar disc, due to the alignment of limb darkening and gravity

<sup>1</sup> <http://cdsarc.u-strasbg.fr/viz-bin/Cat?II/300>

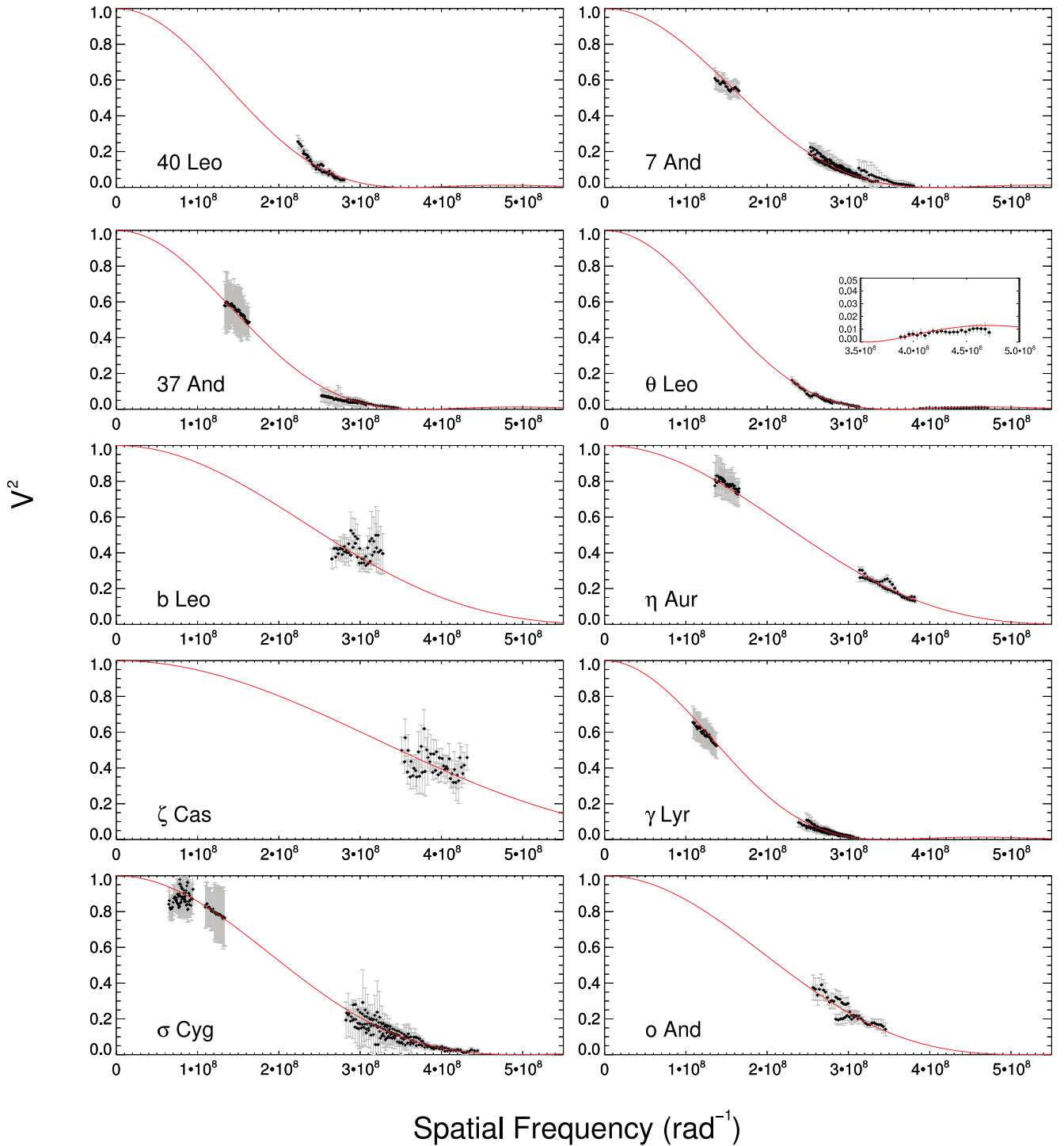


**Figure 1.** Squared visibility versus spatial frequency (defined as projected baseline divided by wavelength) for all stars in our sample. The red solid lines show the fitted limb-darkened disc model. Error bars for each star have been scaled so that the reduced- $\chi^2$  equals unity.

darkening, similar to that observed in other objects (for example, the widely studied case of the AOV fast rotator Vega; Aufdenberg et al. 2006; Peterson et al. 2006; Monnier et al. 2012).

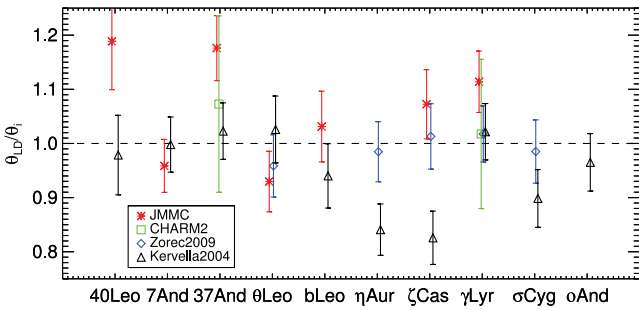
### 3.2 Bolometric fluxes

We have computed the bolometric flux,  $F_{\text{bol}}$ , for all the targets in our sample by fitting the observed absolute SED to grids of ATLAS9 model atmospheres of solar metallicity computed by Castelli &

Kurucz (2003). The fit requires collection of available photometry in the *Hipparcos* ( $H_p$  bandpass), Tycho ( $B_t V_t$ ), Johnson ( $UBVRI-JHK$ ), Geneva ( $UBB1B2V$ ), WBVR (WBVR) and Stromgren ( $ubvy$ ) photometric systems. For the bright objects in our sample, 2MASS  $JHK_s$  photometric measurements are generally saturated, and therefore are not suitable for our purpose, with the sole exception of *b Leo*, for which no other near-infrared colours were found. Photometry longward of near-infrared passbands was not included, as they are frequently affected by infrared excess with non-stellar origin.

**Table 4.** Summary of observations included in this work and measured angular diameters.

ID	Name	HD	$N_{V2}$	Baselines	$\mu_R$	$\theta_{UD}$ (mas)	$\theta_{LD}$ (mas)	$\theta_{V-K}$ (mas)
<i>a</i>	40 Leo	HD 89449	46	E2W1	$0.48 \pm 0.04$	$0.706 \pm 0.026$	$0.731 \pm 0.030$	$0.747 \pm 0.012$
<i>b</i>	7 And	HD 219080	207	W1W2, E2W1, S1W2, S2W1	$0.44 \pm 0.04$	$0.622 \pm 0.006$	$0.648 \pm 0.008$	$0.649 \pm 0.013$
<i>c</i>	37 And	HD 5448	115	W1W2, E2W1, S2W1	$0.43 \pm 0.03$	$0.678 \pm 0.012$	$0.708 \pm 0.013$	$0.692 \pm 0.013$
<i>d</i>	$\theta$ Leo	HD 97633	69	E2W1, S1E1	$0.39 \pm 0.03$	$0.710 \pm 0.023$	$0.740 \pm 0.024$	$0.721 \pm 0.017$
<i>e</i>	b Leo	HD 95608	46	E2W1	$0.38 \pm 0.03$	$0.416 \pm 0.016$	$0.430 \pm 0.017$	$0.456 \pm 0.009$
<i>f</i>	$\eta$ Aur	HD 32630	115	W1W2, S2W1	$0.26 \pm 0.03$	$0.444 \pm 0.011$	$0.453 \pm 0.012$	$0.539 \pm 0.010$
<i>g</i>	$\zeta$ Cas	HD 3360	46	S1E1	$0.26 \pm 0.03$	$0.305 \pm 0.010$	$0.311 \pm 0.010$	$0.376 \pm 0.009$
<i>h</i>	$\gamma$ Lyr	HD 176437	161	W1W2, W1E2, S1W2	$0.34 \pm 0.03$	$0.729 \pm 0.008$	$0.753 \pm 0.009$	$0.738 \pm 0.016$
<i>i</i>	$\sigma$ Cyg	HD 202850	368	W1W2, S2W1, S2E2W2	$0.35 \pm 0.04$	$0.511 \pm 0.014$	$0.527 \pm 0.016$	$0.588 \pm 0.013$
<i>j</i>	o And	HD 217675	46	E2W1	$0.31 \pm 0.03$	$0.494 \pm 0.012$	$0.508 \pm 0.015$	$0.526 \pm 0.011$

**Figure 2.** Fractional differences  $\theta_{LD}/\theta_i$  between angular diameters measured with PAVO and diameters determined using colour–surface brightness relation (JMMC catalogue and Kervella relation; Lafrasse et al. 2010; Kervella et al. 2004), SED fits (Zorec et al. 2009) and direct interferometric measurements collected in the CHARM2 catalogue (Richichi et al. 2005).

Half the stars in the sample have spectral types earlier than A0, implying surface temperatures in excess of 10 000 K. Therefore, these objects radiate pre-dominantly in the ultraviolet. In order to improve the fit of the emergent flux in the ultraviolet region, we have included coadded low-resolution flux-calibrated ultraviolet spectra (in the 1150–1980 Å and 1850–3350 Å ranges) retrieved from the *International Ultraviolet Explorer (IUE)* archive. To avoid occasional flux miscalibration close to the edges of the spectral range covered, we have considered only the 1200–1900 Å and 1900–3300 Å regions.

All photometric data have been corrected from interstellar reddening using the maps of Drimmel et al. (2003) and the extinction

description presented in Fitzpatrick (1999). In the particular case of the highly reddened  $\sigma$  Cyg, we have used the individual interstellar extinction curve presented in Wegner (2002). Photometry was calibrated in flux (using filter responses and zero-points from Kornilov, Mironov & Zakharov 1996; Bessell, Castelli & Plez 1998; Gray 1998; Cohen, Wheaton & Megeath 2003; Bessell & Murphy 2012) and subsequently fitted to the grid of theoretical line-blanketed ATLAS9 spectra, interpolating in both  $T_{\text{eff}}^{\text{model}}$  and  $\log g$  model parameters. The code can also estimate the reddening correction, yielding to  $E(B - V)$  values similar to those mentioned above. Table 5 shows the estimated bolometric fluxes,  $F_{\text{bol}}$ , computed as the numerical integral of the theoretical spectrum corresponding to the best-fitting model parameters  $T_{\text{eff}}^{\text{model}}$  and  $\log g$  (also listed in Table 5). Uncertainties in the estimated parameters are computed using a synthetic population of  $10^3$  data sets accounting for errors (correlated and uncorrelated) in the photometry used and in its calibration in absolute flux.

Fig. 3 displays plots of the resulting SED fits for the stars in the sample studied. For all the stars, the overall agreement between observed and theoretical fluxes is excellent, both in the ultraviolet and visible/near-infrared regions. The best-fitting physical parameters  $T_{\text{eff}}^{\text{model}}$  and  $\log g$  are also in excellent agreement with spectroscopic determinations, with the only exception of  $\gamma$  Lyr, that shows a  $\log g$  value smaller than the one derived from spectroscopy. Temperature measurements of  $\gamma$  Lyr are widely spread in the range 9346–12715 K (Ammons et al. 2006; Koleva & Vazdekis 2012), with associated  $\log g$  values in the interval 3.5–4.11, that appear abnormally high for a giant star. Despite the fact that the SED-fitting method followed should not be considered accurate enough in terms

**Table 5.** Estimated bolometric fluxes from SED fits of ATLAS9 grids of stellar atmosphere models computed by Castelli & Kurucz (2003), using optical and near-infrared photometry ( $F_{\text{bol}}^{\text{SED}}$ ) and low-resolution *IUE* ultraviolet spectra in *short* (1200–1900 Å) and *long* (1900–3300 Å). The table includes the reddening used for each star, as well as the best-fitting  $T_{\text{eff}}^{\text{model}}$  and  $\log g$  parameter values.

Star name	$E(B - V)$ (mag)	Spectrophotometry		Model fit		$F_{\text{bol}}$ ( $10^{-8}$ erg $\text{cm}^{-2}$ $\text{s}^{-1}$ )
		$N_{\text{phot}}$	$N_{\text{UV}}^{\text{short}} / N_{\text{UV}}^{\text{long}}$	$T_{\text{model}}$ (K)	$\log g$ (cgs)	
40 Leo	$0.004 \pm 0.001$	82	1/1	$5812 \pm 126$	$4.29 \pm 0.29$	$30.9 \pm 0.9$
7 And	$0.006 \pm 0.001$	67	3/-	$7024 \pm 354$	$4.00 \pm 0.17$	$41 \pm 2$
37 And	$0.004 \pm 0.001$	43	1/1	$7577 \pm 291$	$4.00 \pm 1.06$	$80 \pm 5$
$\theta$ Leo	$0.005 \pm 0.001$	65	2/1	$9147 \pm 47$	$3.55 \pm 0.27$	$147 \pm 4$
b Leo	$0.005 \pm 0.001$	50	3/4	$8759 \pm 37$	$3.83 \pm 0.35$	$51.0 \pm 1.2$
$\eta$ Aur	$0.014 \pm 0.001$	85	11/40	$16\,212 \pm 63$	$4.40 \pm 0.30$	$831 \pm 11$
$\zeta$ Cas	$0.04 \pm 0.04$	54	1/4	$18\,562 \pm 151$	$4.02 \pm 0.28$	$693 \pm 20$
$\gamma$ Lyr	$0.017 \pm 0.004$	83	1/1	$9640 \pm 60$	$2.64 \pm 0.35$	$215 \pm 4$
$\sigma$ Cyg	$0.13 \pm 0.05$	78	1/1	$9990 \pm 0$	$1.90 \pm 0.06$	$133 \pm 3$
o And	$0.049 \pm 0.022$	45	13/12	$13\,812 \pm 45$	$3.17 \pm 0.10$	$383 \pm 5$

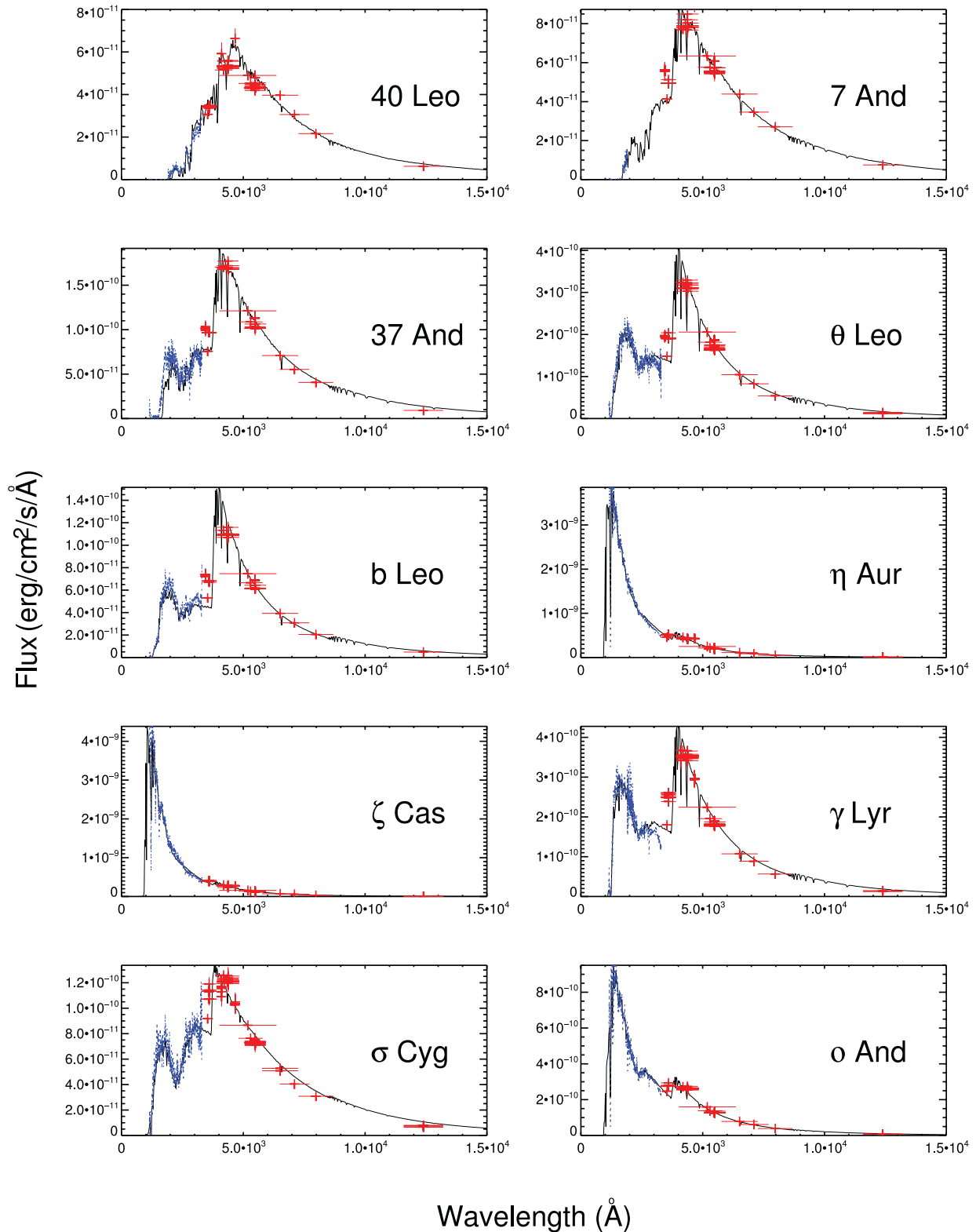


**Figure 3.** SED fits for the stars in our sample. The continuous line represents the best model fitted to the optical and infrared broad-band photometric data (red crosses). The horizontal error bars stand for the effective width of the corresponding broad-band filter. The ultraviolet coadded low-resolution IUE spectra are plotted as blue dots.

of  $\log g$  estimation, the large discrepancy observed seems compatible with a lower expected surface gravity for a giant star than the spectroscopic values (see Table 1). The atmospheric parameters of this object will be discussed again in Section 3.6.

### 3.3 Luminosities, temperatures and linear radii

The combination of the derived values for stellar angular diameters  $\theta_{\text{LD}}$  and bolometric fluxes  $F_{\text{bol}}$  with the *Hipparcos* parallaxes

**Table 6.** Linear radii, luminosities and effective temperatures.

Star	$R (R_{\odot})$	$L (L_{\odot})$	$T_{\text{eff}} (K)$
40 Leo	$1.68 \pm 0.07$	$4.4 \pm 0.9$	$6450 \pm 140$
7 And	$1.71 \pm 0.02$	$7.8 \pm 0.6$	$7380 \pm 90$
37 And	$3.03 \pm 0.11$	$40 \pm 3$	$8320 \pm 150$
$\theta$ Leo	$4.03 \pm 0.10$	$118 \pm 5$	$9480 \pm 120$
$b$ Leo	$1.80 \pm 0.07$	$24.1 \pm 1.4$	$9540 \pm 180$
$\eta$ Aur	$3.64 \pm 0.10$	$1450 \pm 70$	$18\,600 \pm 230$
$\zeta$ Cas	$6.1 \pm 0.3$	$7200 \pm 900$	$21\,500 \pm 400$
$\gamma$ Lyr	$15.4 \pm 0.8$	$2430 \pm 190$	$10\,330 \pm 80$
$\sigma$ Cyg	$50 \pm 9$	$33\,000 \pm 8000$	$10\,940 \pm 180$
$o$ And	$11.5 \pm 1.3$	$5300 \pm 900$	$14\,540 \pm 170$

$\pi$  provides us with estimations of linear radii, luminosities and effective temperatures for the stars in our sample. Measured angular limb-darkened diameters  $\theta_{\text{LD}}$  are transformed into the linear radius  $R$  for each star using the *Hipparcos* (van Leeuwen 2007) parallaxes. The absolute luminosity is computed from the known distance  $d$  to the object and the bolometric flux  $F_{\text{bol}}$  by solving

$$L = 4\pi d^2 F_{\text{bol}}. \quad (3)$$

Finally, the combination of angular diameter  $\theta_{\text{LD}}$  with the estimated bolometric flux  $F_{\text{bol}}$  allows us to measure the effective temperature of a star, defined according to

$$T_{\text{eff}} = \left( 4 \frac{F_{\text{bol}}}{\sigma_B \theta_{\text{LD}}^2} \right)^{1/4}. \quad (4)$$

The values obtained are summarized in Table 6. Fig. 4 displays the results in a Hertzsprung–Russell diagram.

### 3.4 Effective temperature

Fig. 5 displays a comparison of the derived effective temperature values derived from our measurements of  $\theta_{\text{LD}}$  and  $F_{\text{bol}}$  and values

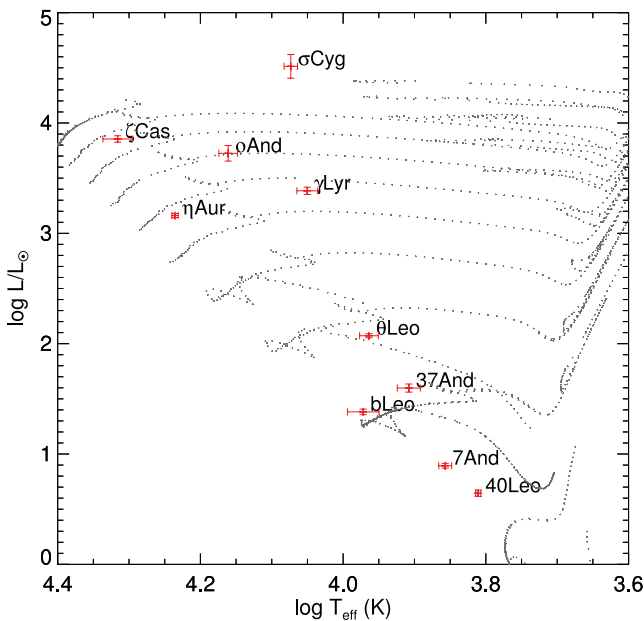


**Figure 4.** Hertzsprung–Russell diagram containing luminosities and effective temperatures derived for the stars in our study (see Table 6). Solar-metallicity PARSEC (Bressan et al. 2012) evolutionary tracks for masses in the range  $1\text{--}10 M_{\odot}$  in steps of  $1 M_{\odot}$  are shown as grey dotted lines.

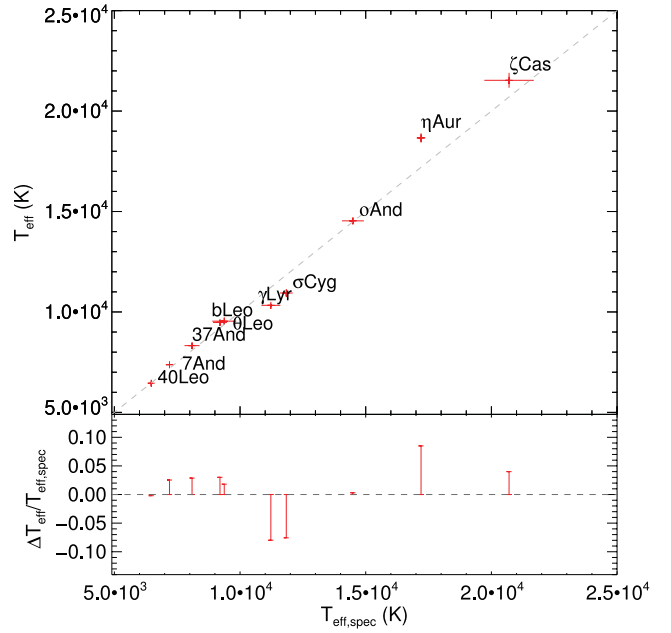


**Figure 5.** Top: comparison of effective temperature estimations derived in this paper with respect to spectroscopic determinations (see Table 1). Bottom: relative difference between both estimations of effective temperature.

determined using spectroscopy listed in Table 1. There is excellent agreement between both sets of measurements, especially for stars of spectral types A0 or later. The average and median deviations are  $\simeq 0.7$  and  $\simeq 2.1$  per cent, respectively, with a scatter of 5 per cent. For main-sequence stars, the scatter reduces to  $\simeq 2.5$  per cent.

Given the effective temperatures in excess of 10 000 K of stars with spectral types earlier than A0, a significant fraction of the total emergent flux is radiated in the ultraviolet region, where systematics caused by limitations of plane-parallel stellar atmosphere models are conspicuous, especially in the case of giants or supergiants. The physical parameters describing the best-fitting model stellar atmosphere do not necessarily represent the best description of the actual physical parameters of the star. Nonetheless, the  $F_{\text{bol}}^{1/4}$  dependence of  $T_{\text{eff}}$  makes the determination of effective temperature to remain robust in spite of the simplified assumptions contained in the stellar atmosphere models used.

Table 7 compares  $T_{\text{eff}}$  derived in our study with results presented in Zorec et al. (2009) for a subset of the five overlapping objects in both samples, with  $T_{\text{eff}} > 9000$  K. The agreement of both sets of measurements is excellent. Small disagreements are likely due to the simultaneous estimation of the photosphere diameter  $\theta^f$ , and the identification of model temperature  $T_{\text{eff}}^{\text{model}}$  and effective temperature  $T_{\text{eff}}$  made in Zorec et al. (2009). In our case, including a direct measurement of the limb-darkened diameter, assumed to represent the photosphere diameter, and estimating  $T_{\text{eff}}$  exclusively from the

**Table 7.** Comparison of derived effective temperatures with results presented in Zorec et al. (2009).

Star	$T_{\text{eff}} (K)$	$T_{\text{eff}}^{\text{Zorec}} (K)$
$\theta$ Leo	$9480 \pm 120$	$9180 \pm 290$
$\eta$ Aur	$18\,660 \pm 230$	$17\,940 \pm 1070$
$\zeta$ Cas	$21\,500 \pm 400$	$21\,850 \pm 1390$
$\gamma$ Lyr	$10\,330 \pm 80$	$10\,000 \pm 350$
$\sigma$ Cyg	$10\,940 \pm 180$	$11\,170 \pm 450$

estimation of the total amount of radiated energy reduce considerably the model dependence of our results, that is limited to the use of theoretical spectra to fit the observed fluxes.

### 3.5 Colour–effective temperature relations

Whereas the empirical temperature scale for giant stars seems to be firmly established with uncertainties under 2.5 per cent (Code et al. 1976; Underhill et al. 1979; van Belle et al. 1999), the same cannot be said for main-sequence stars (luminosity classes IV and V). For those stars in our sample with  $T_{\text{eff}} < 10\,000$  K (spectral types A0 or later), we have contrasted the computed effective temperatures with empirical colour–temperature relations presented in Boyajian et al. (2012a) and van Belle & von Braun (2009) using  $(V - K)$  and  $(B - V)$  colours. Figs 6 and 7 display effective temperature versus  $(V - K)$  and  $(B - V)$  colours for the stars in our sample lying in the temperature range considered, as well as the results presented in

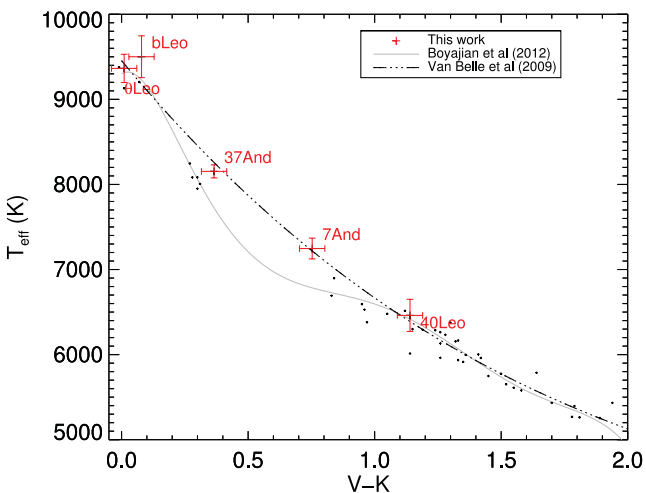


**Figure 6.** Plot of the effective temperature versus  $V - K$  colour for the main-sequence stars in the studied sample with  $T_{\text{eff}}$  below 10 000 K. The solid line represents the empirical relation found in Boyajian et al. (2012a) by means of a sixth-order polynomial fitted to a sample of 44 A- to G-type stars (small black dots). Triple dot-dashed line represents the third-order polynomial fit presented in van Belle & von Braun (2009).

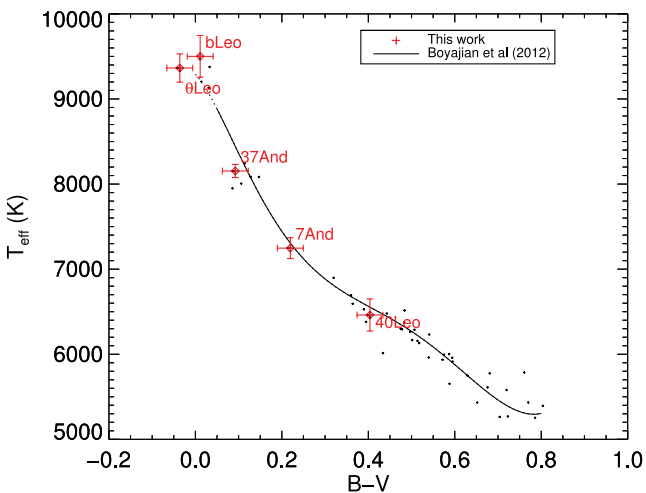


**Figure 7.** Effective temperature versus  $B - V$  colour for the main-sequence stars in the observed sample with  $T_{\text{eff}}$  below 10 000 K. Data from Boyajian et al. (2012a) (small black dots) as well as empirical relation based on a sixth-order polynomial fit (solid line) are also included.

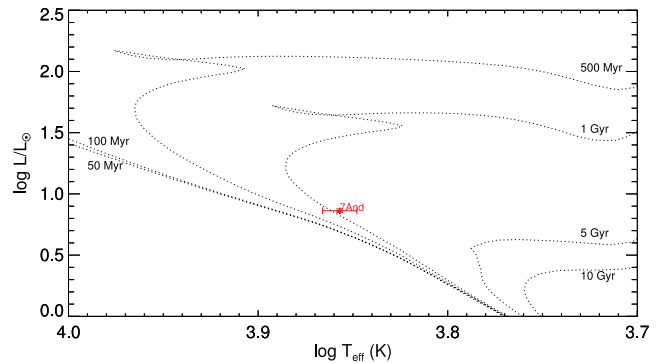


**Figure 8.** Luminosity–temperature diagram showing the isochrones generated for 7 And.

Boyajian et al. (2012a), fitted to a sixth-order polynomial in  $(V - K)$  and  $(B - V)$ , respectively. Fig. 6 adds the empirical relation found by van Belle & von Braun (2009), using a third-order polynomial. Most of the stars in both previous studies are cooler than 7000 K, and both empirical relations nearly overlap in that range of temperatures. The same does not apply for earlier spectral types, as the two fits differ quite significantly between 6500 and 8500 K, where there were no stars in their samples. Three of the stars in our study (37 And, 7 And and 40 Leo) have temperatures within this range. Their location in the  $T_{\text{eff}} - (V - K)$  diagram (Fig. 6) shows strong agreement with the more conservative third-order polynomial relation presented by van Belle & von Braun (2009). On the other hand, our data are fully consistent with the  $T_{\text{eff}} - (B - V)$  sixth-order polynomial relation of Boyajian et al. (2012a) (Fig. 7). Observational effects induced by ubiquitous fast rotation among stars earlier than F6 could explain the disagreement with Boyajian et al. (2012a) sixth-order  $(V - K)$  polynomial relation. Most of the A-type stars studied in that paper show high-projected rotational velocities ( $v \sin i$ ), compatible with fast rotation seen at a lower inclination angle (closer to be equator-on) with respect to the same spectral type stars contained in our sample. Further accurate estimations of  $T_{\text{eff}}$  for a larger sample of main-sequence stars earlier than F5 will significantly improve the empirical temperature scale for these stars.

### 3.6 Masses and ages

We have estimated the stellar masses ( $M_{*,\text{iso}}$ ) and ages for our target sample by fitting the inferred luminosity and effective temperature values to PARSEC<sup>2</sup> isochrones (Bressan et al. 2012). Fig. 8 illustrates the method using 7 And as an example. For each object in our sample, we have computed a grid of isochrones equally spaced in log age (age in years) in the range 1 Myr–10 Gyr, and adopt the best fit to the luminosity and effective temperature computed values. We have assumed solar metallicity for all the stars in the sample. Uncertainties are derived by considering solutions at  $1\sigma$  separation in both luminosity and temperature dimensions. Results obtained are displayed in Table 8.

Using the linear radii estimated from combined measurements of angular diameter and parallax and the spectroscopic determination of  $\log g$ , we can estimate the so-called *gravity mass* (van Belle, Ciardi & Boden 2007) of each object according to

$$g = G \frac{M_{\text{gra}}}{R_*^2}, \quad (5)$$

<sup>2</sup> <http://stev.oapd.inaf.it/cmd>

**Table 8.** Isochrone masses and ages.

Star	$M(M_{\odot})$	Age (Myr)
40 Leo	$1.35 \pm 0.06$	$2630 \pm 210$
7 And	$1.6 \pm 0.1$	$1120 \pm 30$
37 And	$2.21 \pm 0.09$	$724 \pm 21$
$\theta$ Leo	$2.8 \pm 0.1$	$407 \pm 12$
$b$ Leo	$2.11 \pm 0.06$	$195 \pm 15$
$\eta$ Aur	$5.6 \pm 0.1$	$41 \pm 6$
$\zeta$ Cas	$8.96 \pm 0.13$	$22.9 \pm 1.2$
$\gamma$ Lyr	$5.76 \pm 0.13$	$74.8 \pm 5.1$
$\sigma$ Cyg	$11.2 \pm 0.2$	$19.1 \pm 0.6$
$o$ And	$6.5 \pm 0.5$	$52 \pm 9$

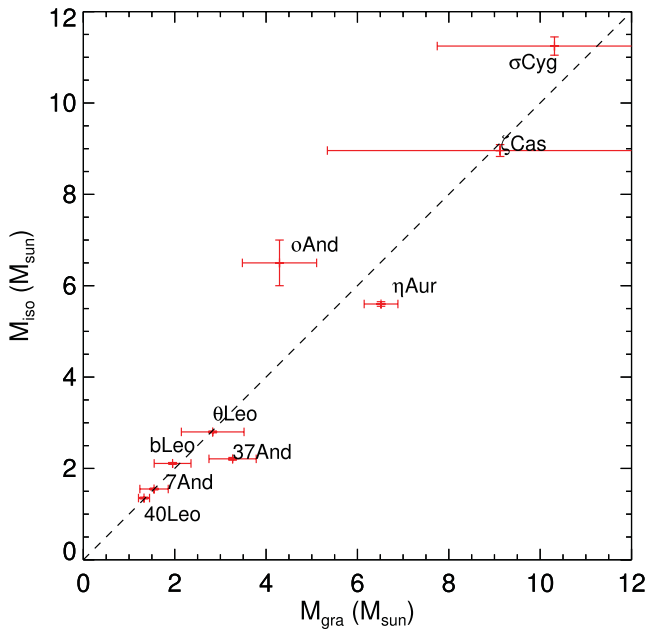


**Figure 9.** Comparison of mass estimations using isochrone fit ( $M_{\text{iso}}$ ) and the gravitational mass  $M_{\text{gra}}$ , computed using spectroscopic surface gravity and linear stellar radii (equation 5). The dashed line represents identity.  $\gamma$  Lyr ( $M_{\text{gra}} = 55 M_{\odot}$ ,  $M_{\text{iso}} = 5.76 \pm 0.13 M_{\odot}$ ) is not shown in the plot.

where  $G$  is the gravitational constant, and  $M_{\text{gra}}$  and  $R_*$  stand for the mass and linear radius of the star considered. Fig. 9 displays the relation between isochrone and gravitational masses. Comparison of masses determined by both methods show a remarkable good agreement for all the objects in the sample except  $\gamma$  Lyr. The reason for the large disagreement in that case is most likely related to the spectroscopic determination of  $\log g$ , since values of 3.5, 4.11 and 3.68 reported by different authors (Balachandran et al. 1986; Prugniel et al. 2011; Koleva & Vazdekis 2012, respectively) are clearly discrepant with the values expected for a B9 giant, which combined with our linear radius estimation result in unphysical gravity mass values of  $M_{\text{gra}} = 27, 41$  and  $111 M_{\odot}$  ( $55 M_{\odot}$  for the mean value  $\log g = 3.81$ ). However, the value of  $\log g$  derived from our SED fit yields a gravity mass value of  $\approx 4.4 M_{\odot}$ , in better agreement with the  $M_{\text{iso}}$  value obtained.

## 4 CONCLUSIONS

We have presented results of a pilot study on a sample of 10 stars (7 main sequence or subgiants and 3 supergiants or giants) with

spectral types between B2 and F6. For all the objects in the sample, we have measured submilliarcsecond angular diameters and bolometric fluxes with an average precision of 2.3 and 2.1 per cent, respectively. Combined with *Hipparcos* parallaxes, we have derived fundamental stellar parameters, linear radii, effective temperatures and luminosities with 8, 3 and 5 per cent average relative uncertainties. Finally, we have fitted PARSEC isochrones to the values of temperature and luminosity found in order to obtain estimates of mass and age for every star in the sample. Our findings can be summarized as follows.

(i) Measured diameters show generally good agreement with predictions based on colour relations or SED fits, as well as with previous interferometric measurements.  $V^2$  data points beyond the first null for  $\theta$  Leo enable simultaneous estimation of diameter and linear limb-darkening coefficient  $\mu$ . Whereas the derived diameter is less than 1 per cent larger than the fixed limb-darkening estimation, the estimated value for  $\mu$  exceeds by  $\approx 20$  per cent the value interpolated in Claret & Bloemen (2011) using stellar atmosphere parameters. This enhanced limb darkening, together with the star's low-projected rotational velocity, suggests that  $\theta$  Leo is in fact a fast-rotating star viewed nearly pole-on.

(ii) We derived bolometric fluxes from SED fits of theoretical ATLAS9 stellar atmosphere models to optical and near-infrared photometric data, as well as including flux calibrated *IUE* ultraviolet spectra, accounting for the effects of interstellar reddening. The mean absolute deviation between derived effective temperatures and estimates using spectroscopy is  $\approx 3$  per cent. The agreement is excellent for main-sequence stars, and only for two of the B giants,  $\gamma$  Lyr and  $\sigma$  Cyg, and the main-sequence star  $\eta$  Aur, the discrepancy is as large as  $\approx 7$  per cent. Comparison with Zorec et al. (2009), for the subset of overlapping objects from our sample reveals excellent agreement in the results of both studies, despite some subtle differences in the modelling assumptions.

(iii) Our derived effective temperatures for A- and F-type stars confirm the sixth-order polynomial ( $B - V$ ) colour–temperature relation presented in Boyajian et al. (2012a). However, there is clear disagreement with their sixth-order ( $V - K$ )–temperature relation, and our data clearly favour the ( $V - K$ ) cubic polynomial presented by van Belle & von Braun (2009). Different inclination angles of the polar axis between Boyajian's sample of A and early F stars with respect to ours, together with the effects of fast rotation in these stars might explain the observed discrepancy. New observations of main-sequence stars in this range of temperature, correcting the scarcity of available data should provide the basis for a more detailed empirical colour–temperature relation.

(iv) The PARSEC model isochrone fit in the temperature–luminosity plane provides mass values that are consistent with the estimated gravitational masses computed from spectroscopically determined  $\log g$ , showing larger discrepancies for larger mass values. The unphysical result obtained for  $\gamma$  Lyr gravitational mass, together with the large scatter in temperature estimations using spectroscopy, questions the accuracy of  $\gamma$  Lyr atmosphere parameters and suggests strong degeneracy between  $\log g$  and  $T_{\text{eff}}$ . Additionally, a  $\log g$  estimation based on the SED fit to spectrophotometric data seems to give a gravity mass that is more consistent with the value obtained by means of the isochrone fitting.

## ACKNOWLEDGEMENTS

The authors would like to thank Chris Farrington, P.J. Goldfinger, Judit Sturman and Jo Cheng for their support during observations

at the CHARA array. This research has made use of the SIMBAD data base and the VizieR catalogue access tool, operated at CDS, Strasbourg, France. Some of the data presented in this paper were obtained from the Multimission Archive at the Space Telescope Science Institute (MAST). STScI is operated by the Association of Universities for Research in Astronomy, Inc., under NASA contract NAS5-26555. Support for MAST for non-*HST* data is provided by the NASA Office of Space Science via grant NAG5-7584 and by other grants and contracts. This publication makes use of data products from the Two Micron All Sky Survey, which is a joint project of the University of Massachusetts and the Infrared Processing and Analysis Center/California Institute of Technology, funded by the National Aeronautics and Space Administration and the National Science Foundation. The CHARA array is funded by the National Science Foundation through NSF grant AST-0606958, by Georgia State University through the College of Arts and Sciences and by the W.M. Keck Foundation. We acknowledge the support of the Australian Research Council. VM is supported by an International Denison Postgraduate Award. D.H. is supported by an appointment to the NASA Postdoctoral Program at Ames Research Center, administered by Oak Ridge Associated Universities through a contract with NASA.

## REFERENCES

- Adelman S. J., 1986, *A&AS*, 64, 173  
 Adelman S. J., 1988, *MNRAS*, 230, 671  
 Adelman S. J., Pintado O. I., Nieva M. F., Rayle K. E., Sanders S. E., Jr, 2002, *A&A*, 392, 1031  
 Allende Prieto C., Lambert D. L., 1999, *A&A*, 352, 555  
 Ammons S. M., Robinson S. E., Strader J., Laughlin G., Fischer D., Wolf A., 2006, *ApJ*, 638, 1004  
 Aufdenberg J. P. et al., 2006, *ApJ*, 645, 664  
 Balachandran S., Lambert D. L., Tomkin J., Parthasarathy M., 1986, *MNRAS*, 219, 479  
 Balona L. A., Dziembowski W. A., 1999, *MNRAS*, 309, 221  
 Bazot M. et al., 2011, *A&A*, 526, L4  
 Berger D. H. et al., 2006, *ApJ*, 644, 475  
 Bessell M., Murphy S., 2012, *PASP*, 124, 140  
 Bessell M. S., Castelli F., Plez B., 1998, *A&A*, 333, 231  
 Blackwell D. E., Lynas-Gray A. E., 1998, *A&AS*, 129, 505  
 Boden A. F., 2003, in Perrin G., Malbet F., eds, *EAS Publications Ser. Vol. 6. Observing with the VLTI*. Cambridge Univ. Press, Cambridge, p.151  
 Boyajian T. S. et al., 2012a, *ApJ*, 746, 101  
 Boyajian T. S. et al., 2012b, *ApJ*, 757, 112  
 Bressan A., Marigo P., Girardi L., Salasnich B., Dal Cero C., Rubele S., Nanni A., 2012, *MNRAS*, 427, 127  
 Castelli F., Kurucz R. L., 2003, in Piskunov N., Weiss W. W., Gray D. F., eds, *Proc. IAU Symp. 210, Modelling of Stellar Atmospheres*. Astron. Soc. Pac., San Francisco, p. 20  
 Che X. et al., 2011, *ApJ*, 732, 68  
 Claret A., Bloemen S., 2011, *A&A*, 529, A75  
 Clark J. S., Tarasov A. E., Panko E. A., 2003, *A&A*, 403, 239  
 Code A. D., Bless R. C., Davis J., Brown R. H., 1976, *ApJ*, 203, 417  
 Cohen M., Wheaton W. A., Megeath S. T., 2003, *AJ*, 126, 1090  
 Cottrell P. L., Sneden C., 1986, *A&A*, 161, 314  
 Cruzalèbes P., Jorissen A., Sacuto S., Bonneau D., 2010, *A&A*, 515, A6  
 Davis J., 1997, in Bedding T. R., Booth A. J., Davis J., eds, *IAU Symp. 189, Fundamental Stellar Properties: the Interaction Between Observation and Theory*. Kluwer, Dordrecht, p. 31  
 Derekas A. et al., 2011, *Sci*, 332, 216  
 Domiciano de Souza A., Vakili F., Jankov S., Janot-Pacheco E., Abe L., 2002, *A&A*, 393, 345  
 Drimmel R., Cabrera-Lavers A., López-Corredoira M., 2003, *A&A*, 409, 205  
 Eggleton P. P., Tokovinin A. A., 2008, *MNRAS*, 389, 869  
 Erspamer D., North P., 2003, *A&A*, 398, 1121  
 Fitzpatrick E. L., 1999, *PASP*, 111, 63  
 Fitzpatrick E. L., Massa D., 2005, *AJ*, 129, 1642  
 Frémat Y., Zorec J., Hubert A.-M., Floquet M., 2005, *A&A*, 440, 305  
 Gardiner R. B., Kupka F., Smalley B., 1999, *A&A*, 347, 876  
 Gies D. R., Lambert D. L., 1992, *ApJ*, 387, 673  
 Gilbocki R., Gnaciński P., 2005, in Favata F., Hussain G. A. J., Battrick B., eds, *ESA SP-560: 13th Cambridge Workshop on Cool Stars, Stellar Systems and the Sun*. ESA, Noordwijk, p. 571  
 Gray R. O., 1998, *AJ*, 116, 482  
 Hanbury Brown R., Davis J., Allen L. R., 1974a, *MNRAS*, 167, 121  
 Hanbury Brown R., Davis J., Lake R. J. W., Thompson R. J., 1974b, *MNRAS*, 167, 475  
 Harmanec P. et al., 1996, *A&A*, 312, 879  
 Hill G. M., Landstreet J. D., 1993, *A&A*, 276, 142  
 Huber D. et al., 2012a, *ApJ*, 760, 32  
 Huber D. et al., 2012b, *MNRAS*, 423, L438  
 Ireland M. J. et al., 2008, *Proc. SPIE*, 701324, 7013  
 Kervella P., Thévenin F., Di Folco E., Ségransan D., 2004, *A&A*, 426, 297  
 Koleva M., Vazdekis A., 2012, *A&A*, 538, A143  
 Kornilov V., Mironov A., Zakharov A., 1996, *Balt. Astron.*, 5, 379  
 Lafrasse S., Mella G., Bonneau D., Duvert G., Delfosse X., Chesneau O., Chelli A., 2010, *Proc. SPIE*, 77344E, 7734  
 Lane B. F., Boden A. F., Kulkarni S. R., 2001, *ApJ*, 551, L81  
 Maeder A., Meynet G., 2000, *ARA&A*, 38, 143  
 Maestro V. et al., 2012, *Proc. SPIE*, 84450G, 8445  
 Mason B. D., Wycoff G. L., Hartkopf W. I., Douglass G. G., Worley C. E., 2001, *AJ*, 122, 3466  
 Mermilliod J.-C., Mermilliod M., Hauck B., 1997, *A&AS*, 124, 349  
 Monnier J. D. et al., 2007, *Sci*, 317, 342  
 Monnier J. D. et al., 2012, *ApJ*, 761, L3  
 Mozurkewich D. et al., 2003, *AJ*, 126, 2502  
 Nieva M.-F., Przybilla N., 2012, *A&A*, 539, A143  
 Olević D., Cvetković Z., 2006, *AJ*, 131, 1721  
 Owocki S. P., Cranmer S. R., Blondin J. M., 1994, *ApJ*, 424, 887  
 Peterson D. M. et al., 2006, *Nat*, 440, 896  
 Pier J. R., Saha A., Kinman T. D., 2003, *Inf. Bull. Var. Stars*, 5459, 1  
 Pourbaix D. et al., 2004, *A&A*, 424, 727  
 Prugniel P., Vauglin I., Koleva M., 2011, *A&A*, 531, A165  
 Richichi A., Percheron I., Khristoforova M., 2005, *A&A*, 431, 773  
 Royer F., Zorec J., Gómez A. E., 2007, *A&A*, 463, 671  
 Smith K. C., Dworetzky M. M., 1993, *A&A*, 274, 335  
 Tassoul J.-L., 2000, *Stellar Rotation*. Cambridge Univ. Press, Cambridge  
 ten Brummelaar T. A. et al., 2005, *ApJ*, 628, 453  
 Tokovinin A. A., 1997, *A&AS*, 124, 75  
 Underhill A. B., Divan L., Prevot-Burnichon M.-L., Doazan V., 1979, *MNRAS*, 189, 601  
 Vakili F., Mourard D., Bonneau D., Morand F., Stee P., 1997, *A&A*, 323, 183  
 van Belle G. T., 2012, *A&AR*, 20, 51  
 van Belle G. T., van Belle G., 2005, *PASP*, 117, 1263  
 van Belle G. T., von Braun K., 2009, *ApJ*, 694, 1085  
 van Belle G. T. et al., 1999, *AJ*, 117, 521  
 van Belle G. T., Ciardi D. R., Boden A. F., 2007, *ApJ*, 657, 1058  
 van Leeuwen F., 2007, *A&A*, 474, 653  
 von Zeipel H., 1924a, *MNRAS*, 84, 665  
 von Zeipel H., 1924b, *MNRAS*, 84, 684  
 Wegner W., 2002, *Balt. Astron.*, 11, 1  
 White T. R. et al., 2013, *MNRAS*, in press  
 Wu Y., Singh H. P., Prugniel P., Gupta R., Koleva M., 2011, *A&A*, 525, A71  
 Yoon J., Peterson D. M., Armstrong J. T., Clark J. H., III, Gilbreath G. C., Pauls T., Schmitt H. R., Zagarelli R. J., 2007, *PASP*, 119, 437  
 Zhao M. et al., 2009, *ApJ*, 701, 209  
 Zorec J., Cidale L., Arias M. L., Frémat Y., Muratore M. F., Torres A. F., Martayan C., 2009, *A&A*, 501, 297